Molecular Crystals and Liquid Crystals
Publication details, including instructions for authors and subscription information:
http://www.tandfonline.com/loi/gmcl16

A New Type of Instability in Nematic CBOOA

M. Cohen [a] , P. Pieranski [a] , E. Guyon [b] & C. D. Mitescu [b c]

[a] Laboratoire de Physique des Solides, Université Paris Sud, 91405, Orsay

[b] Université de Provence, Centre St Jéróme, 13397, Marseille Cédex 4

[c] Pomona College, Claremont, California, 91711

Version of record first published: 28 Mar 2007.

To cite this article: M. Cohen , P. Pieranski , E. Guyon & C. D. Mitescu (1977): A New Type of Instability in Nematic CBOOA, Molecular Crystals and Liquid Crystals, 38:1, 97-108

To link to this article: http://dx.doi.org/10.1080/15421407708084378

Mol. Cryst. Liq. Cryst., 1977, Vol. 38, pp. 97–108

Printed in Holland

A New Type of Instability in Nematic CBOOA†

M. COHEN and P. PIERANSKI

Laboratoire de Physique des Solides, Université Paris Sud, 91405 Orsay

and

E. GUYON and C. D. MITESCU‡

Université de Provence, Centre St Jérôme, 13397 Marseille, Cédex 4

(*Received October 18, 1976*)

A new type of hydrodynamic instability is described for a nematic which does not align in flow (CBOOA above its transition to the smectic A phase). An electric field plays a stabilizing role whereas elastic effects as well as shear lead to instability. The elastic term is shown to play a dominant role even in very large fields, as the instability starts to develop from the boundaries with planar alignment.

1 INTRODUCTION

Flow alignment refers to the possibility in most nematics to get alignment nearly along the velocity field by means of a shear of large enough amplitude. In this paper we present an effect of flow alignment and instability obtained in the complementary class of nematics. The alignment is controlled by the application of an electric field on materials of positive dielectric anisotropy ($\varepsilon_a = \varepsilon_{\parallel}' - \varepsilon_{\perp} > 0$).

The geometry is indicated in the inset of Figure 1. The shear is obtained by sliding the upper glass plate of a plane cell with a constant velocity v_y with respect to the fixed lower one. The liquid crystal is aligned along the velocity axis y by coating the inner walls of the cells with a semitransparent Au electrode evaporated obliquely. An electric field E_z can be applied across the cell using these electrodes.

† Supported in part by an Action Thématique Programmée of the C.N.R.S.
‡ On leave from Pomona College, Claremont, California 91711

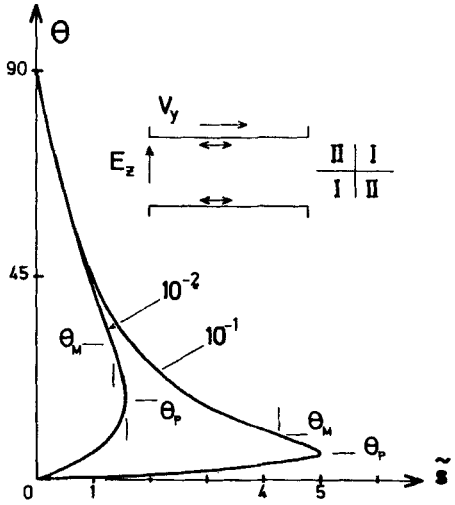

FIGURE 1 Uniform distortion θ as a function of the reduced shear $\tilde{s}$ for two values of the ratio $\alpha_3/|\alpha_2|$, in the case of very large applied electric field. The true limit θ_M is lower than θ_P because of the effect of the boundary layer. (The inset gives the geometry.)

Nematic MBBA will align in a large shear at a small angle θ_0 "against" the flow (in the upper right quadrant, I, in the figure)

$$\tan^2 \theta_0 = \alpha_3/\alpha_2 \tag{1}$$

where α_3 and $\alpha_2(|\alpha_3| \ll |\alpha_2|)$ are viscous torques of negative sign, describing the response to a shear when the director is along y or z.

In its nematic phase, CBOOA (*p*-cyanobenzilidene *p*-octyl oxyaniline) has a coefficient α_3 which goes from a negative value next to the isotropic transition to a positive one over most of the nematic range.[2] A divergence of α_3 (and $\gamma_1 = \alpha_3 - \alpha_2$) is obtained as expected next to the nearly second-order phase transition to the smectic A phase.[3] The coefficient α_2 remains negative and regular. This work will be concerned with CBOOA in the range of temperatures for which α_3 is positive.

For small shears, the director rotates "along" the flow. An equilibrium distortion (in quadrant II of the Figure) can be maintained as long as the splay elasticity (characterized by the Frank constant K_1) can balance the shear torque. It has been shown,[4] however, that for larger shears two different instability modes can be found: A "water-wheel" one with the director rotating in the yz plane of the flow, and an asymmetric one where an x component of the director appears. For larger shears, flow alignment along x can be obtained. For even larger shears, convective instabilities with rolls along the flow will develop if α_3 is not too large. Similar results have been obtained with some

differences (not understood at present) in cylindrical Couette-flow experiments on the same compound.[5]

It is possible to get a flow alignment effect with the director in a stable state of quadrant I (as that obtained for MBBA) if the effect of an electric field is added ($\varepsilon_a > 0$ in CBOOA). The sample is "prepared" as follows: A small shear is applied for a short time in the $-y$ direction; then an a.c. electric field is applied, of high enough frequency to prevent any electrohydrodynamic instability. If E is larger than E_c (the Freedericksz field, $E_c^2 = 4\pi^3 K_1/(\varepsilon_a d^2)$) a single-domain distortion is obtained with the director in quadrant I (thanks to the preliminary application of the shear). If now a shear is applied along $+y$ the effect of the shear will oppose that of the field and a stable alignment angle distribution $\theta(z)$ can be obtained if the shear is small enough. Note, however, that as soon as θ becomes negative (quadrant II)—i.e. for large enough shears—both E and s will act to destabilize the orientation. We will discuss theoretically in II the character of this rather strong and singular instability. A simple treatment neglecting the role of the elasticity fails to predict correctly the instability threshold even in the limit of large fields and shears. It is of interest to note that the elasticity plays a *destabilizing* role in this problem as it tends to reduce the effect of the electric field distortion. Experiments will be presented in Section III.

II THEORY

A Simplified Model

Neglecting the elasticity, the equilibrium distortion is reached when the torque component Γ_y vanishes.

$$\Gamma_y = 0 = s(\alpha_3 \cos^2\theta + |\alpha_2| \sin^2\theta) - (\varepsilon_a/4\pi)E^2 \sin\theta\cos\theta \tag{2}$$

We introduce the reduced shear

$$\tilde{s} = \frac{4\pi|\alpha_2|s}{\varepsilon_a E^2} = \frac{|\alpha_2|sd^2}{K_1\pi^2\mathscr{E}^2} \tag{3}$$

where $\mathscr{E} = E/E_c$. The solution

$$\tilde{s} = \tan\theta/(\varepsilon + \tan^2\theta) \tag{4}$$

is plotted on Figure 1 for two values 0.1 and 0.01 of the parameter $\varepsilon = \alpha_3/|\alpha_2|$. Two equilibrium angles are found for all shears below a critical value:

$$\tilde{s}_P = 1/2\sqrt{\varepsilon} \tag{5}$$

The upper branch is stable whereas the lower one is unstable and will lead to one of the instabilities described in Ref. 4.

The limiting angle θ_P is given by

$$\tan^2 \theta_P = \alpha_3/|\alpha_2| \tag{6}$$

which, rather amusingly, connects with expression (1).

B Role of the elasticity

Experimentally we have never been able to reach this limiting value. This has suggested to us that in all cases the elasticity should be included. The complete equations read

$$K_1 \frac{d^2\theta}{dx^2} = s(\alpha_3 \cos^2 \theta + |\alpha_2| \sin^2 \theta) - (\varepsilon_a/4\pi)E^2 \sin \theta \cos \theta \tag{7}$$

We neglect the anisotropy between bend and splay elasticity, a very good approximation except within 1° of the transition to the smectic A phase in CBOOA.[8] We do not consider the distortion of the electric field caused by that of the director field. This is a more drastic assumption, if we refer to the case of the Freedericksz problem, as the dielectric anisotropy is large[9] ($\varepsilon_a \sim 11 - 5.5 = 5.5$). However, this should not modify too strongly the results for small distortions where the instability is obtained.

We rewrite (7) in dimensionless units as

$$\frac{d^2\theta}{dz^2} = \pi^2 \mathscr{E}^2 [\tilde{s}(\varepsilon \cos^2 \theta + \sin^2 \theta) - \sin \theta \cos \theta]$$

$$= \frac{d}{d\theta}(p^2/2) \tag{8}$$

with

$$z = x/d \qquad p = d\theta/dz.$$

We use the boundary conditions $\theta_{(z=1/2)} = 0$ and, as a consequence of the problem's symmetry, $p_{(z=0)} = 0$ and $\theta_{(z=0)} = \theta_m$ the maximum distortion angle.

We carry out the integration of (8) to obtain

$$p^2 = \pi^2 \mathscr{E}^2 [F(\tilde{s}, \theta_m) - F(\tilde{s}, \theta)]$$

where

$$F(\tilde{s}, \theta) = \sin^2 \theta - \tilde{s}[(1 + \varepsilon)\theta - (1 - \varepsilon)\sin \theta \cos \theta] \tag{9}$$

The formal solution is then completed in terms of the same boundary conditions by taking

$$p = -\pi\mathscr{E}\sqrt{F(\tilde{s}, \theta_m) - F(\tilde{s}, \theta)} \qquad (z \geqslant 0) \tag{9a}$$

whence

$$\pi\mathscr{E}z = \int_{\theta}^{\theta_m} d\theta[F(\tilde{s}, \theta_m) - F(\tilde{s}, \theta)]^{-1/2} \tag{10}$$

where θ_m is defined implicitly by expressing $\theta_{(z=1/2)} = 0$.

The formula can be corrected to take into account the anisotropic elasticity (with $\eta = (K_3 - K_1)/K_1$)

$$\pi\mathscr{E}z = \int_{\theta}^{\theta_m} d\theta[(1 + \eta \sin^2 \theta)/\{F(\tilde{s}, \theta_m) - F(\tilde{s}, \theta)\}]^{1/2} \tag{10a}$$

We can gain significant insight into the nature and the range of solutions given in (10) by looking at Eq. (9) and the function $F(\tilde{s}, \theta)$ plotted in Figure 2 for increasing values of shear. The function displays a negative minimum for a value θ_1 and a maximum for an upper value θ_2. Interestingly, the values θ_1 and θ_2 are the solutions of the simplified model discussed above.

We find, however, that Eq. (9) which results from the presence of elasticity, no matter how weak, always modifies the possible solutions by restricting the allowable values θ_m to a range $(\theta_0 \leqslant \theta_m \leqslant \theta_2) - \theta_0$ being the non-zero intercept of $F(\tilde{s}, \theta)$ on the horizontal axis. This lower limit ensures that the quantity $[F(\tilde{s}, \theta_m) - F(\tilde{s}, \theta)]$ will be positive at $\theta = 0$. Consequently $\tilde{s}$ is restricted to values $\tilde{s} \leqslant \tilde{s}_M$ with the maximal value corresponding to $F(\tilde{s}, \theta)$ tangent to the horizontal axis. In the latter case, the angle $\theta_m = \theta_M$ at which this occurs is the solution of

$$\tan \theta_M = (1 + \varepsilon)\theta_M \tag{11}$$

leading to

$$\tilde{s}_M = \tan \theta_M/(\varepsilon + \tan^2 \theta_M) \tag{11a}$$

This value is always smaller than the value $\tilde{s}_P$ given by (5) (for small ε, $\tilde{s}_M = \sqrt{3}/4\sqrt{\varepsilon}$). While this difference is only of order 20%, it translates into a significant change in the limiting angle θ_M as can be seen on Figure 1 where both limits are indicated.

The complete solutions to Eqs. (10) have been obtained by numerical integration. A typical result for $\eta = 0$ (which is correct not too close to the second order transition to the smectic A phase, $T_{SN} \sim 83°$) is given for $\varepsilon = 0.064$ on Figure 3, where the maximum distortion angle is given as a function

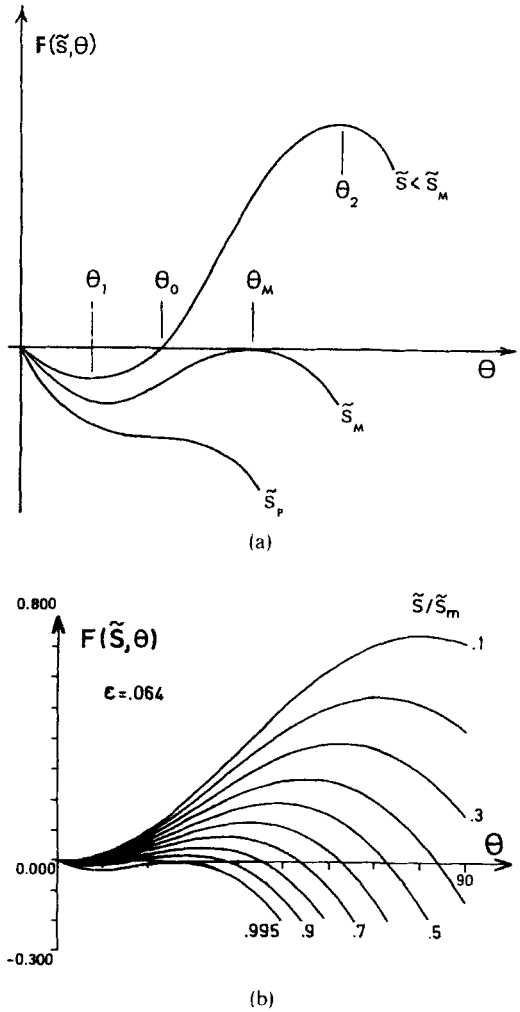

FIGURE 2 (a) Qualitative representation of the function $F(\tilde{s}, \theta)$ indicating its form for the limiting shears $\tilde{s}_M$, $\tilde{s}_P$ and illustrating specific values of θ_m discussed in the text; (b) Calculated values of $F(\tilde{s}, \theta)$ for various values of the reduced shear $\tilde{s}$. Only those choices of θ_m are allowed for which $F(\tilde{s}, \theta_m) \geq F(\tilde{s}, \theta)$ throughout the range $0 \leq \theta \leq \theta_m$.

of the reduced field E/E_c. The curve $\tilde{s} = 0$, without shear, would correspond to the usual Freedericksz one and extrapolates to zero for $\mathscr{E} = 1$. For large electric fields, increasing the shear from zero leads to a decrease of θ_m to the limiting value θ_M on the dotted curve. For fields $\mathscr{E}$ smaller than about 2 the solutions are double-valued. In "normal" experiments where s is increased at constant $\mathscr{E}$ or $\mathscr{E}$ is decreased at constant s, an instability will be reached before

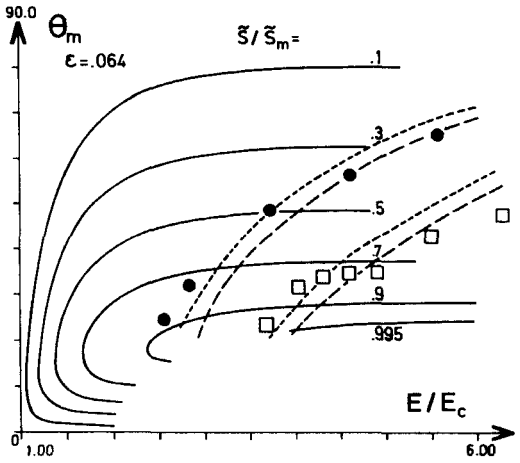

FIGURE 3 The maximum distortion angle θ_m at the center of the cell given as a function of the reduced field $\mathscr{E} = E/E_C$ for various values of the ratio $\tilde{s}/\tilde{s}_M$ (0.1 to 0.995). The points are experimental values obtained at constant shear: $s = 0.95\ s^{-1}$ (squares) and $0.48\ s^{-1}$ (circles). The broken curves correspond to constant shear $s \propto \tilde{s}E^2$. The limiting angle, defined in Eq. (11a), is $\theta_M \sim 20°$.

the lower branch can be entered. The nature of the lower branch and of the transition around the point of vertical slope has not been completely elucidated at the moment, and it is not known whether the lower branch is stable with respect to small perturbations. This could be checked experimentally keeping θ_m constant and increasing s and $\mathscr{E}$ simultaneously (this is difficult to obtain with our set-up where the shear can be applied only for a limited time).

Figure 4 gives the dependence of the distortion with z starting from the center of the cell for two values of reduced field. On the larger field curve one sees the existence of a boundary layer next to the plate where the distortion angle changes rapidly. Its thickness is of the order of the Freedericksz coherence length given by $\xi = d/\pi\mathscr{E}$.

It is the effect of the distortion angle, smaller than θ_m, in this region, no matter how thin it is, which will induce the transition below the limiting value $\tilde{s}_P$ (Eq. 5). Note the inflection very near the limit $\tilde{s}_M$ (for $\tilde{s} = \tilde{s}_M$ the slope $p = d\theta/dz$ is zero on the boundary plates).

III EXPERIMENTS

Two cells of thickness $d = 200\mu$ and 300μ were used. Detailed descriptions of the geometry of the shear flow cell can be obtained from other references.[10] The alignment and distortion were characterized by the formation of the conoscopic image of a strongly converging monochromatic beam ($\lambda = 0.63\mu$)

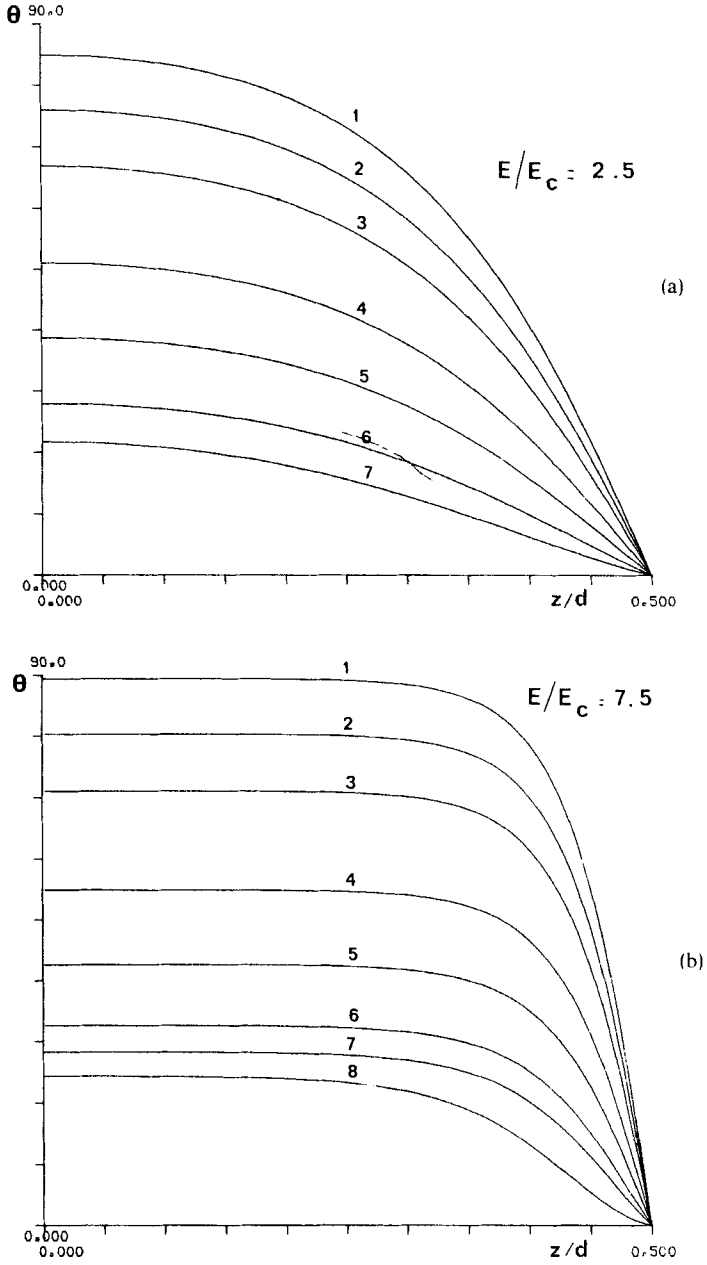

FIGURE 4a and 4b Profile of the distortion angle θ across the half width of the cell ($z = 0$ corresponds to the center), for two values of the reduced field E/E_C. Curves 1 to 8 correspond to increasing shears ($\bar{s}/\bar{s}_M = 0.01, 0.1, 0.2, 0.4, 0.6, 0.8, 0.9, 0.995$).

incident on the cell. A photocell detecting the variation of birefringence along the direction z perpendicular to the cell was coupled either to a recorder for slow enough motion of interference fringes or to a storage oscilloscope if the measurements are done in the presence of large shear and electric fields. The simplest measurement used the following method:

When a given stable distortion is attained, if one suppresses at the same time E and s, one follows the relatively slow (governed by elasticity only) relaxation of the distortion to the planar state. From the numer of fringes N passing in front of the cell, the theoretical estimate of the shape of the distortion profile in the presence of E and s (as given in Figure 4), and the birefringence, one can estimate the initial value of the maximum distortion angle θ_m.

Preliminary measurements are done without shear. From the linear extrapolation of N to zero when E decreases towards E_c one gets the Freedericksz threshold. We obtain a critical voltage $V_c \sim 1.1$ volt independent of thickness. This value is only weakly increasing as the transition to smectic A is approached, as the splay elasticity does not become critical at the transition. However, the slope of the linear variation of $N(V)$ decreases strongly in the vicinity of this transition, anticipating the "ghost transition" effect in the smectic A range.[6] A value of the ratio K_3/K_1 can be obtained from the slope. Our determinations agree with those of Grüler[8]. However, as the slope measurement which characterizes the bend-elasticity (K_3) divergence is less accurate than the threshold measurement used by Grüler in a homeotropic sample, we will use his results here.

In large fields, the count of fringes saturates at a maximum value $\mathcal{N} = (n_e - n_0)d/\lambda$. This value can be obtained from the linear extrapolation of $N(1/E)$ to $1/E = 0$.[7] From this determination we obtain a birefringence only weakly temperature dependent.

Figure 5 gives an experimental determination of the stability curve of a 300μ thick nematic layer next to the inversion temperature where $\alpha_3 = 0$. The electric field E has been kept constant ($V = 8$V) and the shear is varied. The value for $s = 0$, $N = 62$, is close to the limiting value $N = 65$ as $\mathscr{E}$ is large (~ 7). We indeed find that N decreases as the shear increases, in agreement with variations of Figures 1 and 2. The instability manifests itself by our not being able to get any stable fringe pattern when a large enough shear is applied after the initial application of the field (as described in I). In the unstable range we do observe that the conoscopic image moves past the planar image. Then we obtain in most experiments the asymmetric instability with the conoscopic image tilting in the direction of the shear and out of the plane of symmetry. In some instances we have also obtained the water-wheel instability with a count of fringes corresponding to a complete turn of the director. However, this depends on the excellent alignment of the director

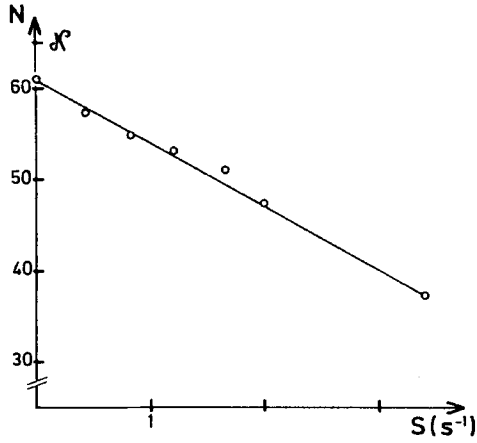

FIGURE 5 Number of fringes counted upon the suppression of both field and shear starting from a stable distortion in quadrant I, displayed as a function of shear. The initial electric field is kept constant ($\mathscr{E} = 7.3$). The observed limiting shear has substantial uncertainty due both to the time of application of the shear and to the presence of defects or dust particles in the flow field.

along the flow axis, and an independent study considering in particular the role of defects introduced would certainly be of interest. Coming back to Figure 5, we see that the variation next to the higher shear, where we could obtain a stable state, does not show any curvature, unlike the variation given in Figure 1. An accurate determination of the threshold is not easy because the dynamics is very slow when the distortion angle becomes of the order of the limiting value, and one must wait a time comparable with the available displacement time of the cell. Also, the role of defects or of dust particles is very crucial in this region and it is generally observed that the instability nucleates at the back of dust particles present in the flow. Clearly, the presence of boundary layers at such particles can play a role analogous to those on the side walls. This is particularly important if homeotropy is reached locally on such grains. The order of magnitude of this threshold agrees with that deduced from (11) or (5) using the elastic constant deduced from the electric field measurement, and α_2 and α_3 values obtained from the results of Refs. 2 and 3. The difference of limiting shear value of 30% between the two theoretical forms cannot be resolved from this experiment due to the experimental uncertainty coming from the dynamic aspect of the measurement. A quantitative comparison between experiment and theory is given in Figure 3 for a 300μ thick film. The temperature of the experiment $T = T_{SN} + 8.5°$ corresponds to the ratio $\varepsilon = 0.064$.[2] In this experiment, the shear values have been kept constant ($s = 0.95$ and $0.48\ s^{-1}$) and the electric field has been varied. The total number of fringes for homeotropy is $\mathscr{N} = 95$. From the

experimental value N we can deduce θ_m from

$$N/\mathcal{N} = 1.21\theta_m^2 A(\theta_m) \tag{12}$$

The factor A includes both the effect of the geometry of the distortion and of the birefringence. It has been calculated numerically and is given in the diagram of Figure 6 as a function of $\tilde{s}$ and $\mathscr{E}$. Using this abacus, we get experimental values of θ_m which are plotted as a function of field on Figure 3. On the same curve, we have plotted calculated curves corresponding to $\tilde{s}\mathscr{E}^2 =$ 11.95 and 13.60 for the smaller shear, and 23.90 and 27.20 for the larger one. The ratio of 2 between the calculated values as well as the overall agreement of shape is in agreement with the model. From the values of $\tilde{s}\mathscr{E}^2$ and the

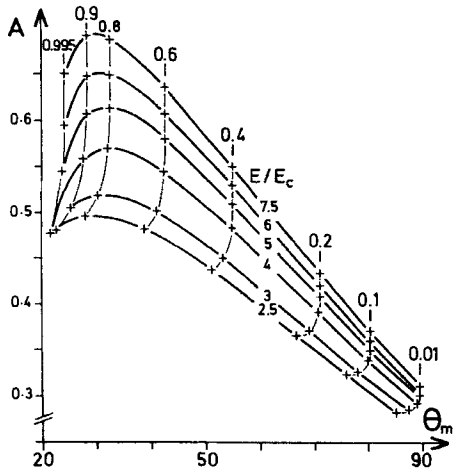

FIGURE 6 The factor $A(\theta_m)$ in Eq. (12) includes both the geometrical effect of the distortion profiles of Figure 4 and the birefringence. This abacus displays lines of constant field $\mathscr{E}$ as well as constant reduced shear $\tilde{s}/\tilde{s}_M$.

experimental shear we obtain, using Equation (4), a value of the ratio $\alpha_2/K_1 = 33 \pm 0.3 \times 10^{-6}$ cgs which is consistent with a determination $K_1 = 1 \pm 0.1 \times 10^{-6}$, obtained from the Freedericksz threshold[8] and from the value[3] of χ_a and $\alpha_2 = -0.37 \pm 0.05$ (deduced from $\gamma_1 = 0.40 \pm 0.05$ [3] and a ratio $\alpha_3/|\alpha_2| = 0.064$ [2]). We also see that the limit angle $\theta_m \sim 25°$ (corresponding to a number of fringes $N = 10 \pm 1$ for both shears) agrees better with the determination $\theta_M = 20°$ than with that $\theta_P \sim 14°$ given by the simplified model. The scatter in the experimental points and, in particular, the shift between the points for small and large angles, is an effect of the dynamic character of the transition and of the rather subjective appreciation of equilibrium angle when slow changes are obtained. An independent dynamic study is clearly desirable.

IV CONCLUSION

We have analyzed in this work a new type of instability where the role of the boundary-layer elasticity plays a dominant destabilizing role even in large fields. The dynamics of the transition next to the limiting angle deserves more consideration. In particular it looks that, for shears slightly above the threshold $\tilde{s}_M$ and below $\tilde{s}_P$ where we know that no stable state is obtained in the first quadrant, we can obtain nevertheless a fairly long-lived state when the distortion passes through the angle characterized by the angle θ_m. Such a situation is reminiscent of the case of first-order transition where unstable states close to the limit of metastability are characterized by a time-dependent profile with an intermediate state of large lifetime (small imaginary part of the energy).[11]

This experiment can also be used to determine within the same experimental realization a number of parameters characteristic of the inelastic behavior, namely K_1. K_3, α_2, α_3 (γ_1 if the dynamic study is performed), ε_a, $n_e - n_0$. This can be of interest as two of these variables have a critical behavior next to the smectic A transition if materials which decompose with time (as CBOOA does) are studied.

Acknowledgements

We thank M. Grenet for help in the preliminary part of the experimental work, the Orsay chemists for the synthesis of CBOOA, Messrs. Le Berre and Hareng for communications of unpublished results.

References

1. F. M. Leslie, *Arch. Rat. Mech. Anal.*, **28**, 265 (1968). The notations used are those of de Gennes (*The Physics of Liquid Crystals*, Oxford University Press, 1974) to whom we refer for the discussion of the viscoelastic behavior of nematics.
2. P. Pieranski and E. Guyon, *Commun. on Phys.*, **1**, 49 (1976).
3. H. Gasparoux, F. Hardouin, M. F. Achard, and G. Sigaud, *J. Phys.*, **36**, Cl, 107 (1975).
4. P. Pieranski, E. Guyon, and S. A. Pikin, *J. Phys.*, **37**, C13 (1976).
5. P. E. Cladis and S. Torza, *Phys. Rev. Lett.*, **35**, 1283 (1975).
6. A. Rapini, *J. Phys.*, **33**, 237 (1972).
7. H. Deuling, to be published as a chapter in supplement to *Solid State Physics*.
8. L. Cheung, R. B. Meyer, and H. Grüler, *Phys. Rev. Lett.*, **31**, 349 (1973).
9. M. Hareng, private communication.
10. P. Pieranski and E. Guyon, *Phys. Rev. A.*, **9**, 404 (1974).
11. K. Binder, *Phys. Rev. B.*, **8**, 3423 (1973).